RESEARCH ARTICLE

INTERNATIONAL RESEARCH JOURNAL OF MULTIDISCIPLINARY TECHNOVATION

Asian Research Association

DOI: 10.54392/irjmt24325

# Spectral Properties of Silica Sol, Gel and Aerogel Doped with Metal Ions and Laser Dyes

**Mohammed A. Anaz [a], Israa F. Al-sharuee [b, *]**

[a] Department of Physics, College of Science, Al-Anbar University, Al-Anbar, Iraq

[b] Department of Physics, College of Science, Mustansiriyah University, Baghdad, Iraq

*Corresponding Author Email: i81f54@uomustansiriyah.edu.iq

DOI: https://doi.org/10.54392/irjmt24325

Received: 01-01-2024; Revised: 27-04-2024; Accepted: 14-05-2024; Published: 30-05-2024

**Abstract:** For the purpose of this investigation, a lower hydrophobic silica aerogel was synthesized. Following doping with metal ions (CuCl) and AgCl, as well as laser dyes fluorescein and coumarin, the produced silica was transformed from a sol-gel to an aerogel throughout the process. Under the conditions of ambient pressure drying, the structure of silica aerogel has been described. Further, the modification began with Sol and culminated in the production of aerogel with the use of trimethylchlorosilane (TMCS) and hexane as solvent components. In the research, the influence of doping with dyes and metal ions on morphological and physical characteristics was investigated. The results showed that the aerogel that was generated after being doped with metal ions and laser dyes had superior physical qualities, including reduced volume shrinkage and decrease in density. The technique of spectroscopy for the purpose of analyzing the variance in chemical bonding, Raman and fluorescence were applied. field emission scanning electron microscopy (FESEM) and surface topography examination (AFM) were used to establish the hydrophobicity property. Fourier transform infrared spectroscopy (FTIR) was used to confirm the hydrophobicity property. Furthermore, the findings demonstrated that aerogels had outstanding performance in a wide variety of physical attributes. The Raman spectra of samples of sol, gel, and aerogel showed a greater degree of variation in the areas of the peaks and the manner in which they were distributed on the spectrum. Additionally, the homogeneities and nanostructures manifested themselves more prominently.

**Keywords:** Doped aerogel, Hydrophobic silica, Laser dyes, Metal ions

## 1. Introduction

Aerogels are well-defined as the gels that contain a microporous solid in which the dispersed phase is gas [1, 2]. Also, the aerogels can be liquid-air gels are those in which the solid network decreases only little when the liquid is replaced by air [3]. The sol-gel process is used to create aerogels, and it entails the chemical transformation of a liquid system (sol) into a gel phase. Silica is often derived from precursors like tetramethoxysilane (TMOS) and tetraethoxysilane (TEOS) [3, 4]. Due to the importance of temperature and pressure interactions in determining the final product's qualities, gel drying is a crucial stage. Aerogel is the name given to the dried product after the solvent has been extracted from the gel structure and the network has been filled with air [5, 6]. As is well known, silica are the main sources for fabricating the aerogels, especially when the synthetic polymers, and other organic precursors are developing sources. As is well known, silica, alumina and carbon, are the main sources for fabricating the aerogels, especially when the synthetic polymers, biopolymers, and other organic precursors are emerging sources. In comparison to other lightweight materials, silica aerogels stand out due to their exceptional qualities. These include a low density (0.003-0.5 g/cm$^3$), a high porosity (80-99.8%), a high specific surface area (500-1200 m$^2$/g), a low index of refraction (1.05), a very high thermal insulation value (0.005 W/mK), and a low index of refraction (1.05 [7]. These porous materials are the result of drying wet gels in a variety of ways (supercritical drying, fluidized bed drying, ambient pressure, atmospheric pressure, etc.) that preserve the nanostructure and prevent the pores from collapsing. The unique properties of silica aerogels are attributed to its remarkable network structures formed through clustered silica nanoparticles. The practical interest in the silica aerogels originates from their potential in the fields of catalysis, waveguides, drug delivery, thermal insulators, storage devices, supercapacitors, radiation detectors, sensor material, etc. [8, 9]. Their low heat conductivity and density make them attractive for a wide range of aerospace uses [10]. These aerogels are desirable as thermal insulation for windows and Cerenkov radiators because they are lightweight, delicate, and have weak mechanical

strength [11]. They have always been considered a promising option for usage in a variety of waste-related, medicinal, gas-sensing, and air-purifying processes [12]. The microporosity of silica aerogels, which supplies the bulk vacuum space filled with air, is responsible for their distinctive properties. Bead-like secondary particles, made out of silica primary particles, create a pearl-necklace-like skeletal network. A 3D network with a pearl necklace topology is formed when parent silica particles coalesce and join to generate secondary particles linked by a siloxane bond (Si-O-Si) [13]. The particles have a dendritic shape, which should lead to the development of a porous structure with pores of between 5 and 100 nm in diameter. Although silica aerogels are quite strong, their restricted mechanical qualities mean they have limited use. Therefore, their potential for practical usage is enhanced by the addition of reinforced micro/nanoscopic materials such as carbon nanotubes, fibers, or nanoparticles as a second phase. For instance, when combined with water-soluble polymers, these silica aerogels create composites that provide thermo-responsive hydrogels with thermal and mechanical characteristics that mirror those of the integrated polymer [14, 15]. Tuning characteristics in this way has the potential to produce porous, very lightweight materials with exceptional mechanical strength and toughness. There has been a lot of progress in this area, and now the modified silica aerogels have features and structural qualities that make them stand out from the native ones. Absorption of hazardous compounds and nanoscale liquid transport are only two examples of the many potentials uses that have been found for functionalized versions of their surfaces in the chemical and biological industries [16]. Because of their high porosity, pore accessibility, and surface area, silica aerogels are exciting and attractive in science and industry. Because of their high porosity, they tend to be somewhat fragile. Ding, H Min, at. al, Results showed that the gel disadvantaged around 393 K and polymerized to create complex silicate around 833 K while heating. It presented steadily intense luminescence because of part of doped europium reduction spontaneously. We found that the modified-on silica gel doped with europium lowered the luminescent transfer temperature about 500K [17]. S Ai, Y Chen, at. al, according to the findings, the nitrogen-doped graphene aerogel that was generated by employing aniline as the nitrogen source exhibits a high nitrogen content, a strong mechanical strength, and outstanding electrical conductivity. Additionally, it has a large specific surface area. In light of these characteristics, the nitrogen-doped graphene aerogel that has been developed demonstrates great performance in the electrochemical detection of dopamine in the presence of uric acid and ascorbic acid. In light of the fact that aerogels may be processed in an easy and scalable manner, the nitrogen-doped graphene aerogels that have been described are anticipated to have potential uses in sensors and other related devices [18]. SB Singh, M De According to the findings of the research, alumina-based templates are just as excellent as, if not better than, carbon-based templates for the synthesis of templated carbon [10]. G Liu, Y Liu According to the findings, composite aerogels also have great performance in a multitude of physical qualities, including superior mechanical property (12.5 MPa) and good heat insulation (0.0225 W/ (m K)). The fact that the thermal conductivity coefficients of silica aerogel monoliths varied from 0.0220 to 0.0340 W/ (m K) as the temperature climbed from 0 to 550 degrees Celsius demonstrated an effective heat wadding effect throughout the thermal process [19]. X Wu, Y Sun, at. al, Results from this study suggest that carbon aerogel-supported single atoms can be used as a dual-functional nanozyme for the construction of low-cost, high-performance dual-signal readout platforms for glucose detection [20]. S Jaiswal, K Bhattacharya, at. al, the results demonstrated that the Ag8 doped coating has the strongest antibiofilm property among the Ag coumarin complexes. After 4 days of exposure to bacterial growth, XPS verified the continued existence of silver at the coated surface in the nanoparticulate form (Ag (0)). Studies comparing the cytotoxicity of various coatings found that the Ag-complex coatings were safer than the AgN coating. In conclusion, a sol-gel matrix containing Ag-coumarin complexes may provide safe, antimicrobial surfaces [21]. S Daneshmand-Jahromi, D Karami *et. al*, the results demonstrated that the proper support can stabilize Cu dispersion, intensify the redox degree of OCs at high temperatures, and strengthen the distribution of Cu on the surface of the support [11]. Ahmed S.S *.et. al*, study the hydrophobic property of the aerogel might potentially be increased by using the doping approach. When compared to undoped aerogel, doped aerogel has a lower density, which indicates that its particles are smaller and that its surface is more uniform [22]. This study discussed the prepare aerogels doped with metal ions and laser dyes at room temperature and ambient pressure and analyzed their Raman, fluorescence, and absorption spectra in sol, gel, and aerogel forms. the findings and discussion of the inquiry into the alteration of structural characteristics of samples.

## 2. Materials and Methods

### 2.1 Materials

Tetraethylorthosilicat (TEOS, 98 %) SigmaAldrich, Germany. Trimethylchlorosilane (TMCS, > (97%) TCI Japan. Hexane (> 98%), from (Belgium). Ethanol from Schariau (Spain) > (98%) Hydrochloric acid (35-38%), from ThomaBaker. Ammonia from CDH. Copper chloride, (0.084g) CuCl) of copper chloride are dissolved in 50 ml ethanol, and add (0.71g) of silver chloride (Ag Cl). (0.166g) (0.074g) fluorescein and coumarin are dissolved in(50ml) ethanol. Molecular weight of coumarin (146.144g/ml). molecular weight of

fluorescein (332.31g/ml) molecular weight (170.51g) (CuCl) and molecular weight (169.88g) (AgCl).

Firstly, Condensed silica (CS) was synthesized by dissolving TEOS in ethanol at a molar ratio of 20:40, stirrer for 15 minutes. In the first step of the process, the dopant materials were combined with condensed (10 ml) and placed under a magnetic stirrer for 15 minutes. Finally, the sol was converted to a gel by adding catalyzed by the base (0.5M $NH_4OH$). This gel is aged for 2 hours after being prepared for 15 minutes, and then cleaned 3 times every 24 hours in ethanol. After baking the gel for 24 hours at (60˚C), the surface was modified by applying a solution of TMCS (7.5ml) in (30ml) hexane, letting it sit at room temperature for 24 hours, and then exchanging the hexane for 4 hours, then dried at room temperature by progressively increasing the oven temperature by 20 degrees, up to a total of 180 degrees.

### 2.2 Methods and Characterization

Raman Spectroscopy is a chemical analysis technique which provides detailed information about chemical structure, phase and polymorphic, crystallinity and molecular interactions. The use of steady-state fluorescence spectroscopy and its effect on the spectral properties. UV-VIS spectrophotometer was used in this work to record the transmittance of the aerogel samples. FT-IR spectrophotometer was used to collects high spectral resolution data for samples of aerogel over the spectral range from 400 $cm^{-1}$ to 4000 $cm^{-1}$. Atomic force microscopy (AFM) is a powerful microscopy technique. It is used to acquire high-resolution images at the nanoscale to better understand the properties of matter. The morphology and microstructures of silica aerogels specimens were observed by with a scanning electron microscope (FSEM) in secondary electron mode.

## 3. Results and Discussion

### 3.1 Absorption and Fluorescence examinations

Figures 1 and 2 indicate absorption spectrum the metal ions copper chloride and silver chloride with ultraviolet-visible spectroscopy-Vis spectra collected from 300 to 600nm were analyzed to establish the presence of silver and copper chloride. Absorbance in the sol-phase-grafted gel-phase was measured. There was a sharp increase in absorbance at 270 nm after adding $NH_3OH$, and the fluid soon gelled. a peak at 370 nm. Both the sol and gel phases of silver chloride had maximal absorbances of 270nm and 300nm. The use of reference solutions allowed for the creation of a calibration curve. When metal ions are present in a solution at sufficiently high concentrations, the absorption spectrum displays many peaks.

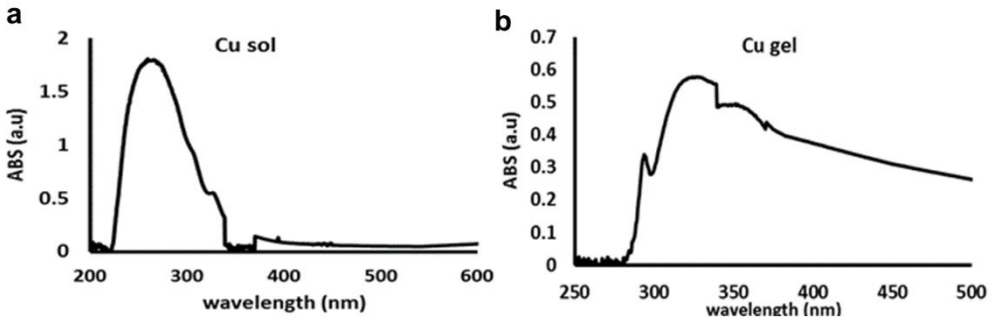


**Figure 1.** The Absorption examines for silica (a):sol (b): gel doped with copper chloride

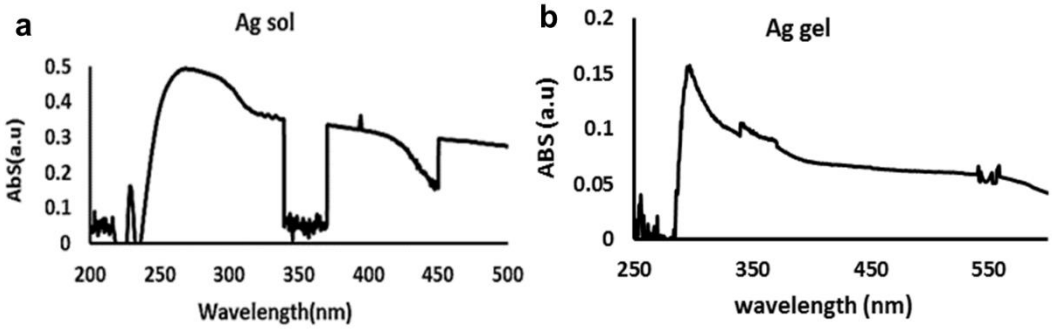


**Figure 2.** The Absorption examines for silica (a):sol, (b): gel doped with silver chloride

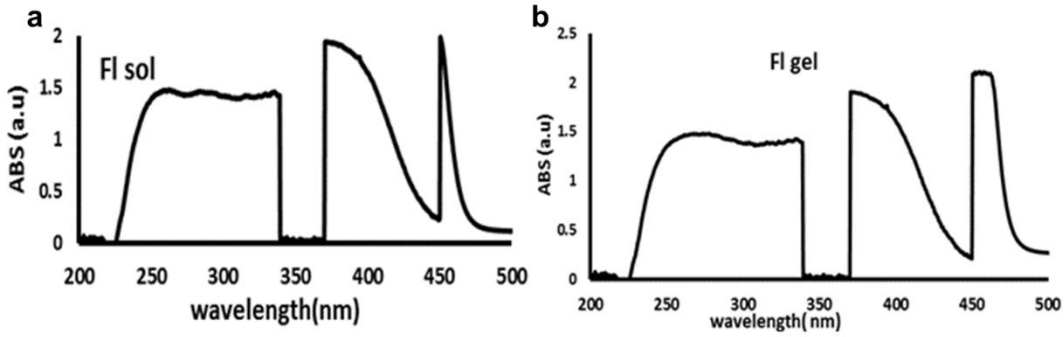


**Figure 3.** The Absorption examines for silica (a):sol, (b): gel doped with fluorescein

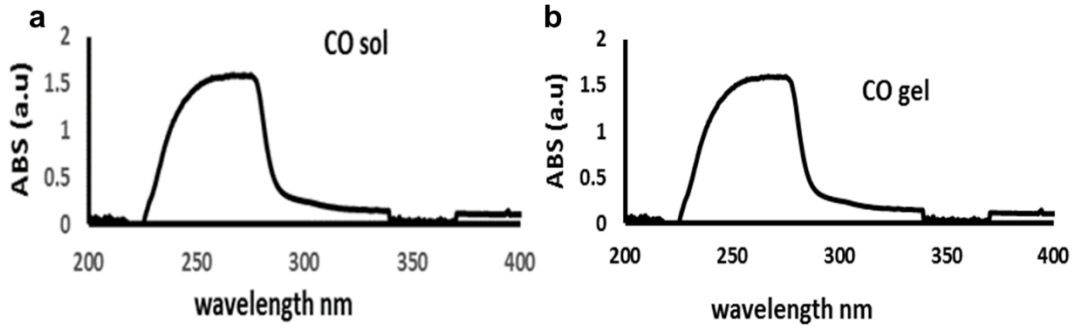


**Figure 4.** The Absorption examines for silica (a):sol, (b): gel doped with coumarin

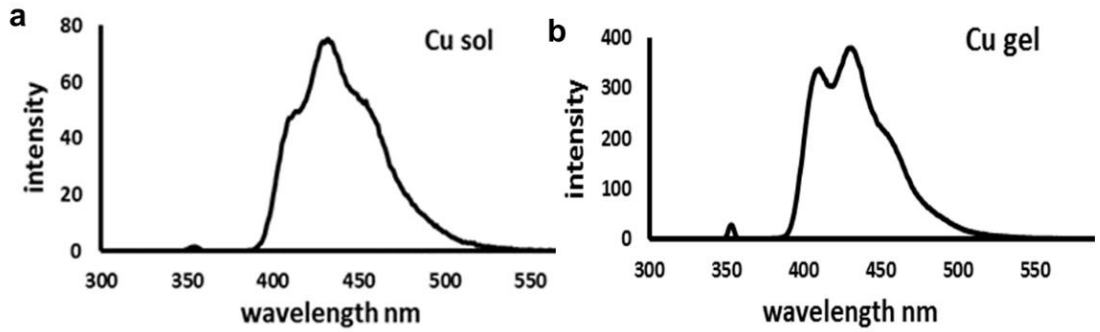


**Figure 5.** Fluorescence examines for silica (a):sol, (b): gel doped with copper chloride

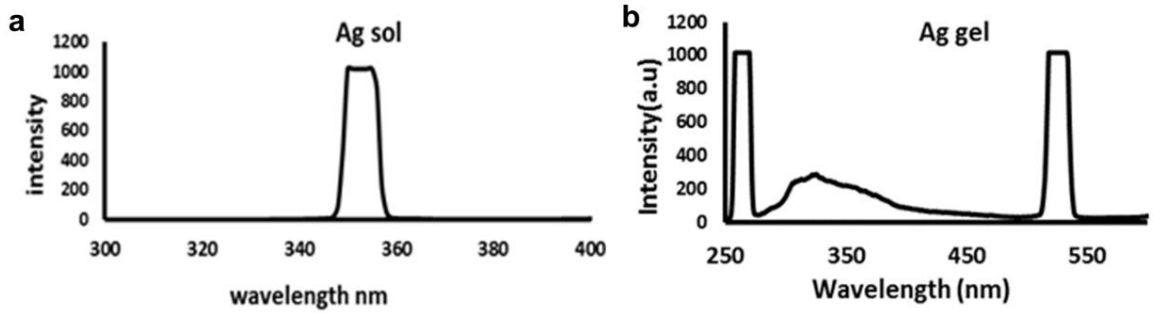


**Figure 6.** Fluorescence examines for silica (a):sol (b): gel doped with silver chloride

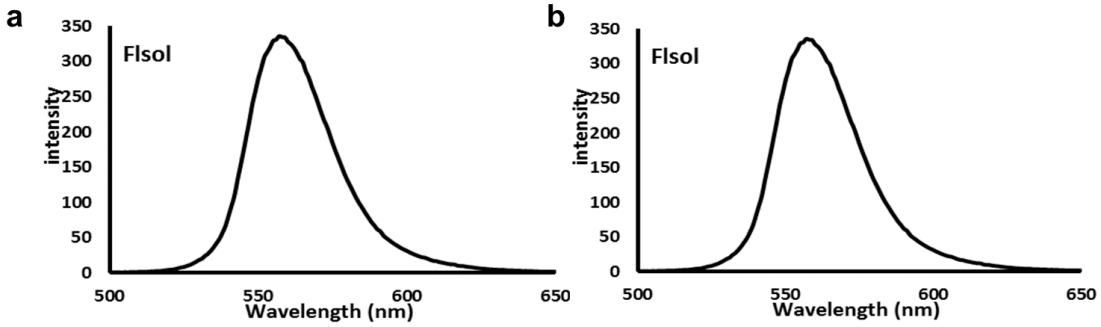


**Figure 7.** Fluorescence examines for silica (a):sol (b): gel doped with fluorescein

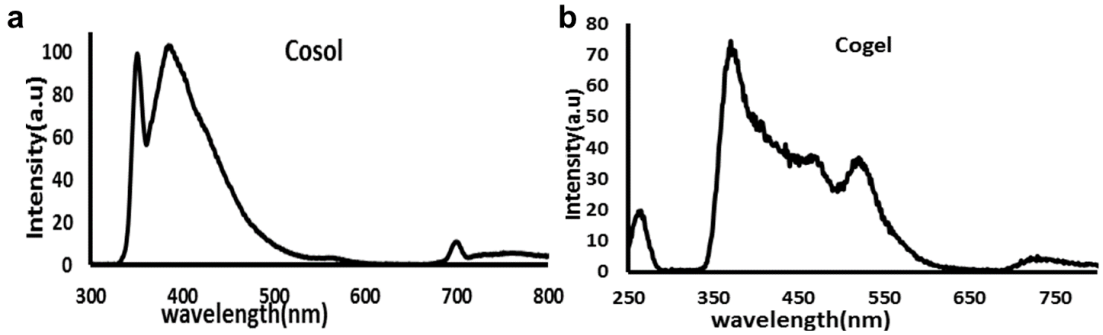


**Figure 8.** Fluorescence examines for silica (a):sol (b): gel doped with coumarin

Higher concentrations create more trapped radiation owing to closer particle closeness; this is because "these are because the absorbance and concentration are closely connected". Since the absorbance of a solution increases in direct proportion to the concentration of that solution, increasing the concentration of the starting substance increases its absorbance as well [23]. Figures 3 and 4 indicate absorption spectrum the coumarin fluorescein in case of coumarin, the peak absorption intensity of each band increased, the absorbance peak at 470nm was detected in the sol phase, and the addition of $NH_3OH$ led to gelation of the solution. The sensor could detect an absorbance peak at 460 nm. The substance gelled after showing an absorbance peak at 280 nm during the sol phase. Absorbance varies with wavelength, peaking at 290 nm. These modifications result from the increased energy level of the dye due to the larger perturbation field acting on the absorbance parameters of the molecules at a wavelength doped with sol-gel dye as the dye concentration [24].

Figs 5 and 6 indicate Fluorescence spectrum the metal ions copper chloride and silver chloride Doped samples exhibit changes in electronic band structure, as shown in the photoluminescence spectra, which are related to the presence of metal ions introduced by crystal defects such as oxygen vacancies. $O_2$ voids improved the efficiency of photogenerated electron-hole separation. Fluorescence has been increasing over time. There is a noticeable rise in fluorescence under constant light. When the sol was lit, showed the highest intensity at the wavelength of at 430 nm; after being converted to a gel, showed the highest intensity at the wavelength of at 450 nm for silver chloride, the highest intensity was in the sol phase of 350nm, and after conversion to gel, the highest intensity was 540nm. These findings point to chemical interactions between the probe particles and the hydroxyl radicals produced on the surface of the sol and gel during the photocatalytic process as the cause of fluorescence. Fluorescent hydroxyl products might also have resulted from the photogenerated holes interacting directly with the probe molecules. There seems to be a lot of photocatalytic activity in the gel. Examining and illustrating the possible reaction process may be done using fluorescence measurement of the hydroxyl products [15]. Figures 7and 8 indicate Fluorescence spectrum for coumarin and fluorescein revealed a distinct peak at 560 nm in the sol phase, and many peaks at 590 nm in the gel phase (due to the gel's higher density). The spectrum widening of silica gel is evident from the image. The gel form with fluorescent exhibits stronger fluorescence than sol form around its peak wavelength of 390nm. Photoluminescence spectra of the doped samples show a broad and intense emission band; this is because the particles in liquids have more freedom to move about randomly than those in solids, so the energy is lost when particles collide, suggesting that the expansion process is of a homogenous kind. Due to the large intermolecular distances in a solid, molecular collisions are very infrequent. [25].

### 3.2 Raman Analysis

Figures 9 and 10 shows the Raman analysis in three different cases sol-gel-aerogel doped with copper and silver chloride respectively. While the main peaks of Raman signified in table 1 and 2 Figures9 and 10 indicate Raman spectrum the metal ions copper chloride and silver chloride in the case of silver chloride, the highest intensity has a wavelength of 178.111 in the sol phase, and after the transition to the gel, a change in intensity occurred, and the highest intensity had a wavelength of 171.947nm.

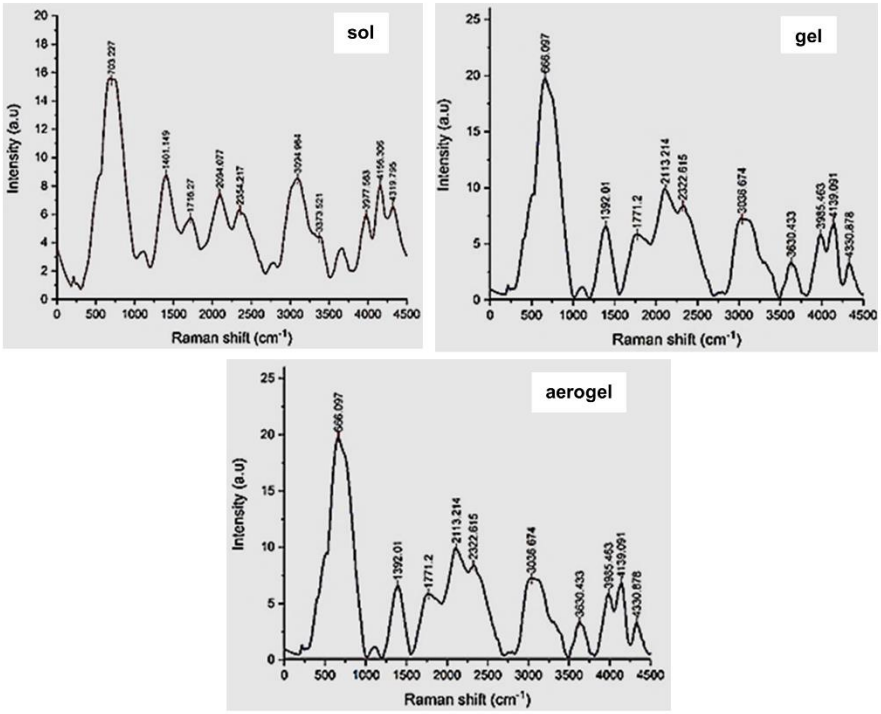


**Figure 9.** Raman analysis of sol- gel-and silica aerogel doped with copper chloride

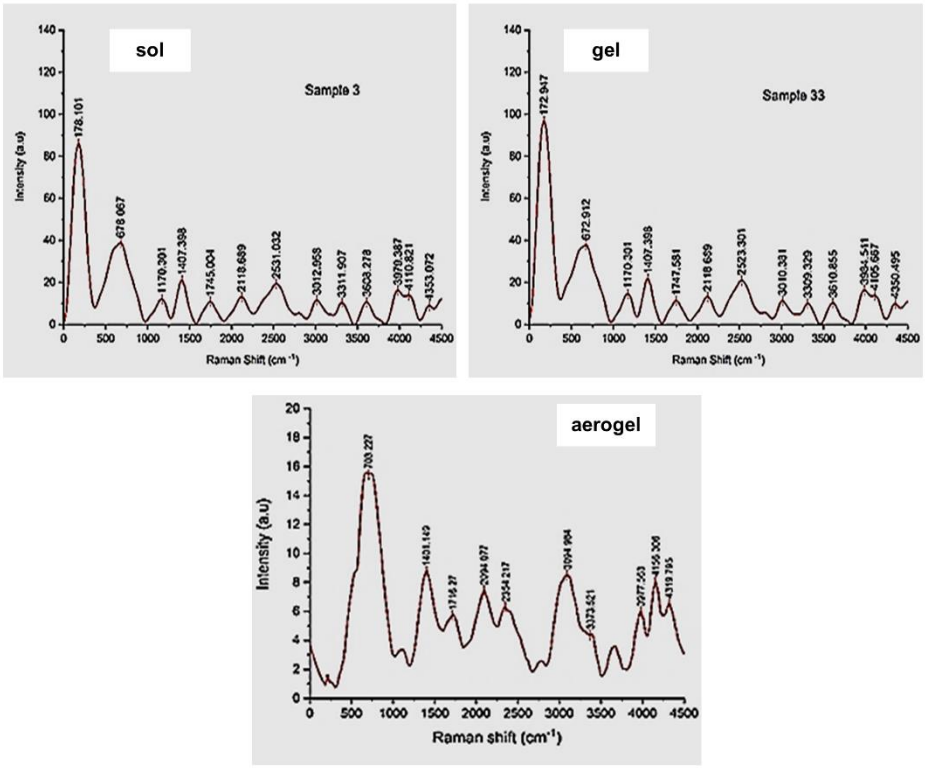


**Figure 10.** Raman analysis of sol- gel-and silica aerogel doped with silver chloride

**Table 1.** The main peaks of Raman analysis

| Sol | | | |
|---|---|---|---|
| X | Y | X | Y |
| 245.33 | 1.66 | 3010.381 | 4.51 |
| 700.33 | 15.3 | 3317.061 | 4.11 |
| 1172.878 | 2.3 | 3610.855 | 5.00 |
| 1412.552 | 9.32 | 3981.964 | 6.86 |
| 1755.312 | 5 | 4115.975 | 7.13 |
| 2123.844 | 8.11 | 4342.764 | 6.19 |
| 2525.878 | 5.53 | | |
| Gel | | | |
| X | Y | X | Y |
| 183.255 | 5.90 | 3007.804 | 12.95934 |
| 666.097 | 18.066 | 3314.484 | 7.65324 |
| 1172.878 | 9.68 | 3605.701 | 13.50612 |
| 1409.975 | 1.33 | 3987.118 | 15.55851 |
| 1755.312 | 9.46154 | 4105.667 | 12.96628 |
| 2123.844 | 12.84857 | 4350.495 | 9.91953 |
| Aerogel | | | |
| X | Y | X | Y |
| 666.097 | 19.74375 | 3036.674 | 7.23027 |
| 1392.01 | 6.58406 | 3630.433 | 3.34193 |
| 1771.2 | 5.86324 | 3985.463 | 5.8486 |
| 2113.214 | 9.85671 | 4139.091 | 6.8149 |
| 2322.615 | 8.41671 | 4330.878 | 3.2936 |

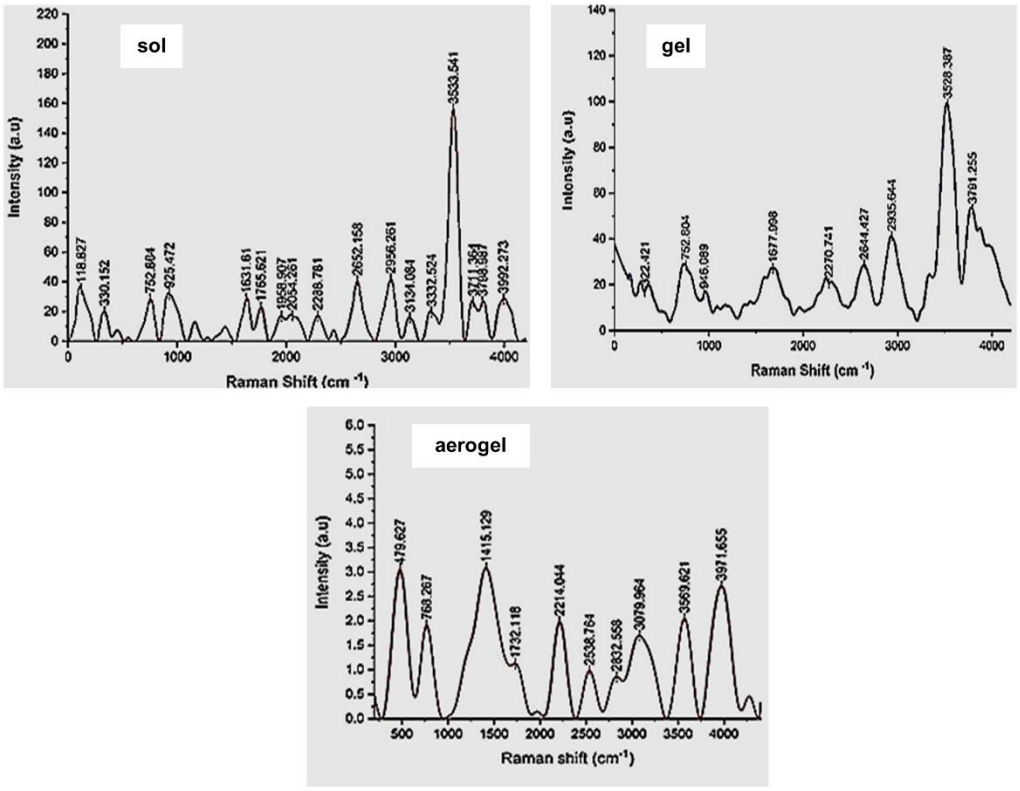


**Figure 11.** Raman analysis of sol- gel-and silica aerogel doped with fluorescein

**Table 2.** The main peaks of Raman analysis

| Sol | | | |
|---|---|---|---|
| X | Y | X | Y |
| 178.101 | 86.14839 | 3012.958 | 11.61914 |
| 678.067 | 38.89121 | 3311.907 | 10.4901 |
| 1170.301 | 12.10675 | 3608.278 | 10.77409 |
| 1407.398 | 21.07558 | 3979.387 | 16.29367 |
| 1745.004 | 10.91559 | 4110.821 | 13.90321 |
| 2118.689 | 13.12174 | 4353.072 | 9.03303 |
| 2531.032 | 19.40828 | | |
| Gol | | | |
| X | Y | X | Y |
| 172.947 | 96.89184 | 3010.381 | 11.32655 |
| 672.912 | 37.77782 | 3309.329 | 10.10434 |
| 1170.301 | 14.61548 | 3610.855 | 10.39258 |
| 1407.398 | 21.83268 | 3984.541 | 16.49185 |
| 1747.581 | 11.37633 | 4105.667 | 13.72377 |
| 2118.689 | 13.27542 | 4350.495 | 9.94842 |
| 2523.301 | 21.07477 | | |
| Aerogel | | | |
| X | Y | X | Y |
| 703.227 | 15.47056 | 3094.984 | 8.53072 |
| 1401.149 | 8.76208 | 3373.521 | 4.38245 |
| 1716.27 | 5.74151 | 3977.563 | 5.9749 |
| 2094.077 | 7.46126 | 4156.306 | 8.06211 |
| 2354.217 | 6.29194 | 4319.795 | 6.53991 |

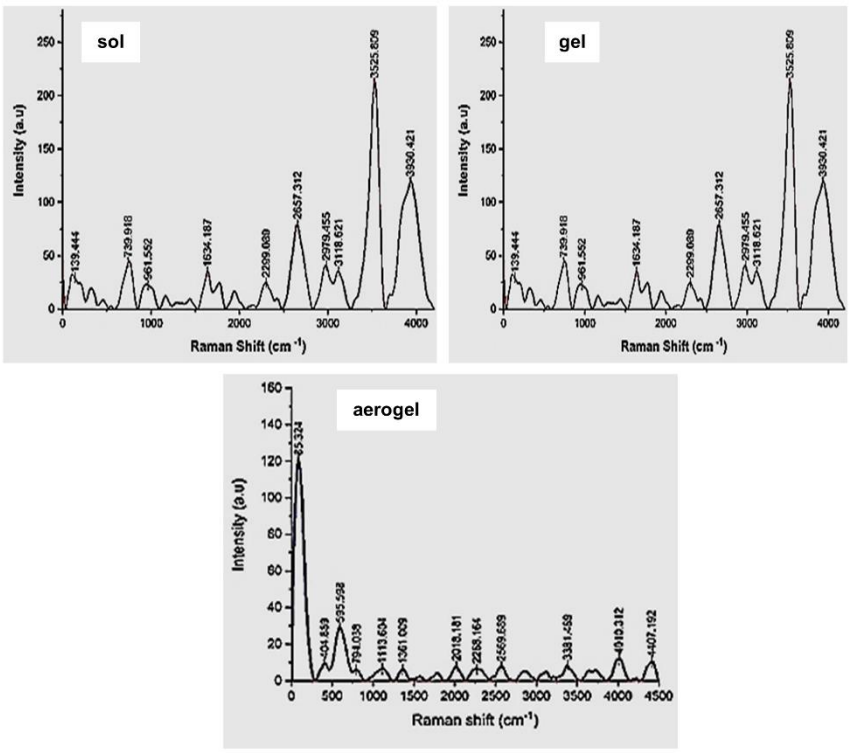


**Figure 12.** Raman analysis of sol- gel-and silica aerogel doped with coumarin

Because of the modification on the surface of the sample used and at different temperatures, a shift occurred in the intensity value, and the highest intensity looked after modifying the surface at the wavelength 703.237 nm. As an initial step, Raman spectra were collected for all the prepared cases. The maximum intensity is at wavelength 180.678nm. Similar Raman domains are seen when TEOS functional groups are present. Next, monitoring of the sol-gel course was achieved in each formulation by following varying Raman signal strengths between the major components [26]. As seen in table 1 and 2 which represented all peaks seemed in Raman spectrum, the maximum intensity of the gel phase at wavelength 183.255 which likes to the ranging vibration of the Si-O-Si bond. In general, it is possible to discriminate the chief districts in Raman of a copper chloride-doped aerogel. The highest intensity seemed at wavelength 666.097-2113.221nm. In there was a change in the Raman spectroscopy. At modified surface with TMCS+ hexane, the strongest peaks appeared at the wavelength 666.197-2114.214nm, where the symmetric extending vibration signified the single type of vibration, and weakest peaks appeared at the wavelength, 3631.433-4329. 878.nm the regular expansion vibration of atoms causes the emergence of weaker peaks [3].

Figures 11 and 12 show the Raman spectrum for aerogel doped with coumarin and fluorescein dyes, the stretching vibrations attributed to Si-O-Si. It was Each of the reactants in sol phase had their Raman spectra taken. The strongest wavelengths are 3526.809 and 3931.421nm. When TEOS functional groups are present, corresponding Raman domains form. The C-O, Si-O, and O-Si-O expansion modes of silicon oxide is all included here. In addition, the Raman spectra of phase gel revealed certain novel peaks associated with the nanocrystalline phase of silicon. Some peaks, however, either maintained or slightly increased their strength. This suggests that TMCS/hexane was used to modify the silica aerogel. The amount of functional group surface modification determines the density of the silica aerogel [27]. The vibration specified by the symmetrical extending tremor produced the aerogel's solidest peaks to form at the wavelength 85.324.-595.598nm after surface modification, while the weakest peaks occurred at the subsequent wavelength 3630.433-4330.878nm. The regular growth vibration of atoms causes the appearance of these weaker peaks. The statistics show that coumarin causes significant variations in fluorescein intensity. Raman spectra were first acquired at the beginning of the process for each sample. The intensity for the sol phase was measured between 3525.809 and 3930.421 nm. After that, the sol-gel procedure was carried out, with the brightest results seen between 3533.54 and 3731.981 nm. The antenna gel that was also prepared with TMCS/hexane exhibited a maximum intensity peak at a wavelength of 85.324-595.598 nm, corresponding to a symmetric stretching vibration, and a minimum intensity peak at the wavelength of 3630.433-4330. 878.nm [28].

### 3.3. FTIR Analysis

The FTIR analysis for silica aerogel doped with CuCl, AgCl, coumarin and fluorescein are shown in figures 13, a, b, c, and d.

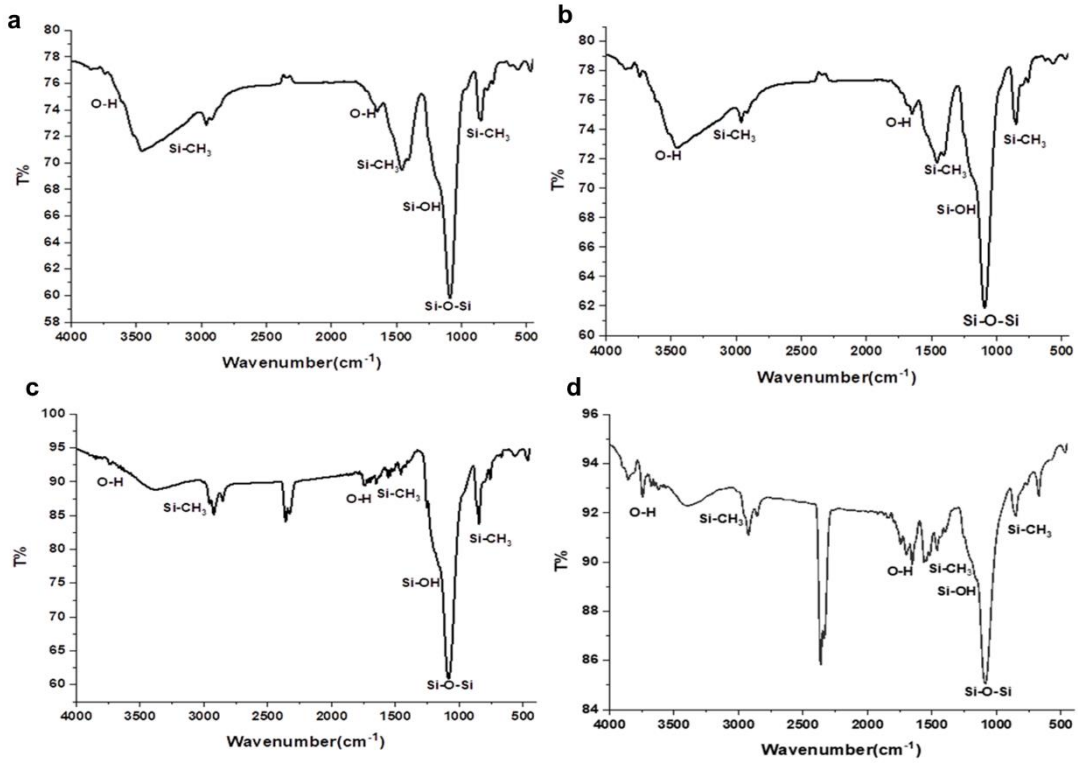


**Figure 13.** FTIR graph of aerogel doped with a: CuCl b: AgCl c: coumarin d: fluorescein

Figures 13 a and b indicates FTIR spectrum the copper and silver chlorides. There is some evidence from the past that implies hydrophilic (alkyl) groups were replaced with hydrophobic (silanol) ones. The Si-O-Si bands, which are present in all samples, peak clearly at 1088 $cm^{-1}$ The decline is visible now [29]. Three bending/stretching peaks, at 33428, 1548, and 1010 cm-1, were identified in Si-$CH_3$. Two more peaks, at 3556 and 1690 $cm^{-1}$, have been associated with the H-OH. Moreover, the pictures reveal a drastic weakening of the Si-OH signal around 1160 $cm^{-1}$. This signal strengthens when metal ions are removed, proving that the TMCS/n-hexane surface modification works. In the case of AgCl, the peaks at 3590 and 1648 $cm^{-1}$ induced by the H-OH bands are less noticeable because the Si-O-Si bands produce significant peaks at 1100 $cm^{-1}$ and 1457 $cm^{-1}$ [30]. Figures 13 c and d shown FTIR spectrum the coumarin fluorescein the hydrophobicity of the silica aerogel powder samples was confirmed using (FTIR). The asymmetric, symmetric, and bending modes of Si-O-Si account for the 1083 cm1,2359 $cm^{-1}$ absorption peaks. Common silica aerogel network architectures include these peaks. Si-C bonding is indicated by the 1260 $cm^{-1}$ and 850 $cm^{-1}$ peaks, whereas the 2960 $cm^{-1}$ and 1600 $cm^{-1}$ peaks are due to C-H stretching. There were no peaks in the spectral distribution of the silica aerogel powder samples at the frequencies associated with the stretching vibration of O-H (3455 $cm^{-1}$and 1635 $cm^{-1}$) and Si-OH (800 $cm^{-1}$). It follows that the TMCS/hexane-modified methyl groups on the silica aerogel's surface rendered it hydrophobic. his suggests that a high concentration of function groups on the surface of the low-density silica aerogel contributes to its improved hydrophobicity [6]. In case of fluorescein When light strikes a molecule, the molecule's vibrations occur in predictable patterns; in the case of coumarin, these patterns are set by the structure of the molecule. Since the silica-containing model has pronounced peaks at 1079 $cm^{-1}$ and 845$cm^{-1}$ respectively, from the Si-O-Si bands, the dip is less pronounced. Si-$CH_3$'s stretching and bending maximum frequencies were 3371 $cm^{-1}$, 1521 $cm^{-1}$, and 844 $cm^{-1}$, respectively. H-OH peaks are also seen at 3644 and 1650 $cm^{-1}$ [3]. In addition, Si-OH might be responsible for the 1160 $cm^{-1}$ nanometer peak, while hydroxide OH in the sample would cause a peak at 3400 $cm^{-1}$ nanometers, although a weak one for the hydrophobic material. When TMCS/hexane is added to the sample's surface, the chemical composition changes, and new peaks appear at the Si-O-Si region that correspond to the silanol group after the hydroxide group has been replaced for the silane functional group [31].

### 3.4. Atomic Force Microscope (AFM)

The atomic force microscopy of silica aerogel doped with metal ions are shown in Figures 14 and 15. Figures 16 and 17 for the dye laser. All figures give a comprehensive description of the surface topography of CuCl and AgCl prepared. The dimensions were described from the two-dimensional images of the surface topography. The roughness factor (where the surface roughness ratio is represented by the value of the mean square root) is crucial since it gives an indication of surface quality and grain growth.

As for the surface roughness, it is measured by the number of protrusions. The greater the number of protrusions, the greater the surface roughness the material has good properties, the surface area is large, and the bumps are nanoparticles. Figures 16 and 17 indicate (AFM) of coumarin fluorescein. The small particles with high stuffing density Surface roughness and the development of agglomerated grains as a function of doping concentration Scan area is (RMS) roughness of Samples. As the Al-mole percentage is increased, the surface quality of the samples improves. The most prominent feature of the graphic is the sheer quantity of tiny particles. also, the aerogel silica gel structure contains nanoscale material that has been grafted onto it. The greater the number of protrusions, the greater the surface roughness the material has good properties.

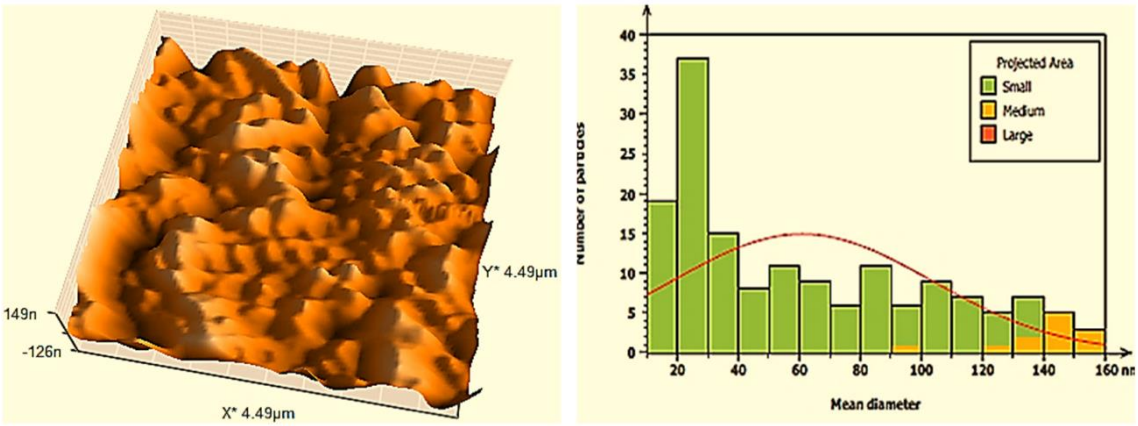


**Figure 14.** AFM image of silica aerogel doped with (CuCl)

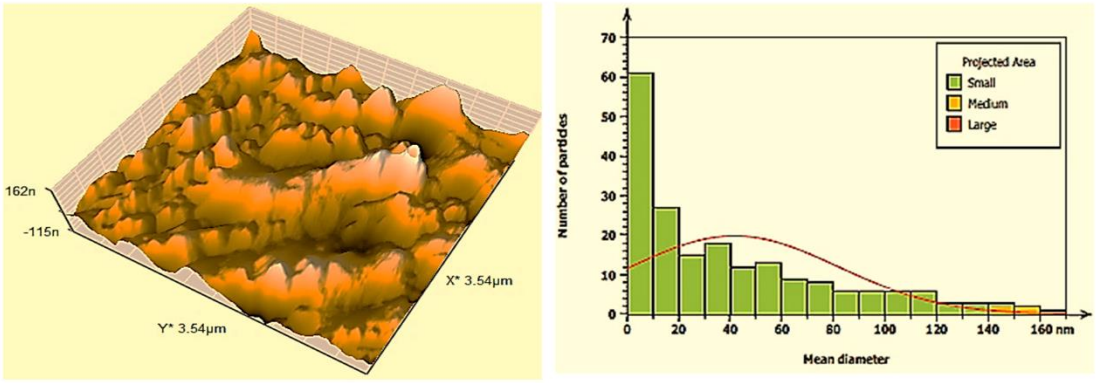


**Figure 15.** AFM image of silica aerogel doped with AgCl

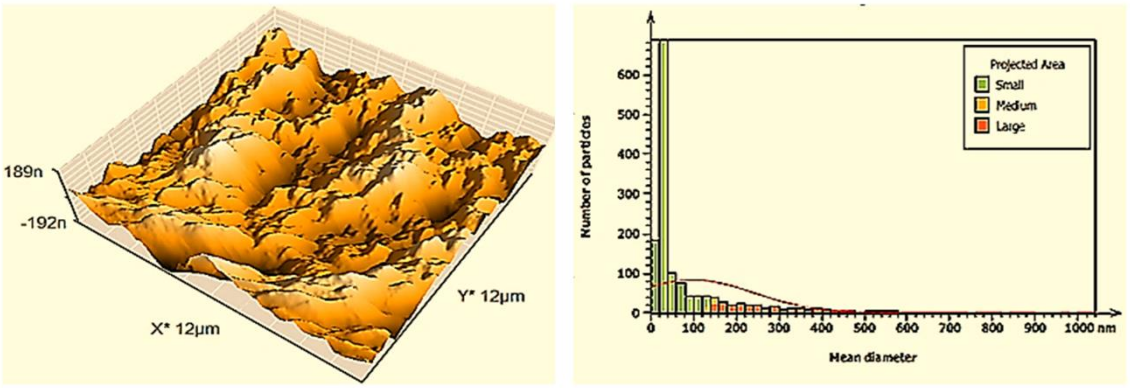


**Figure 16.** AFM image of silica aerogel doped with coumarin

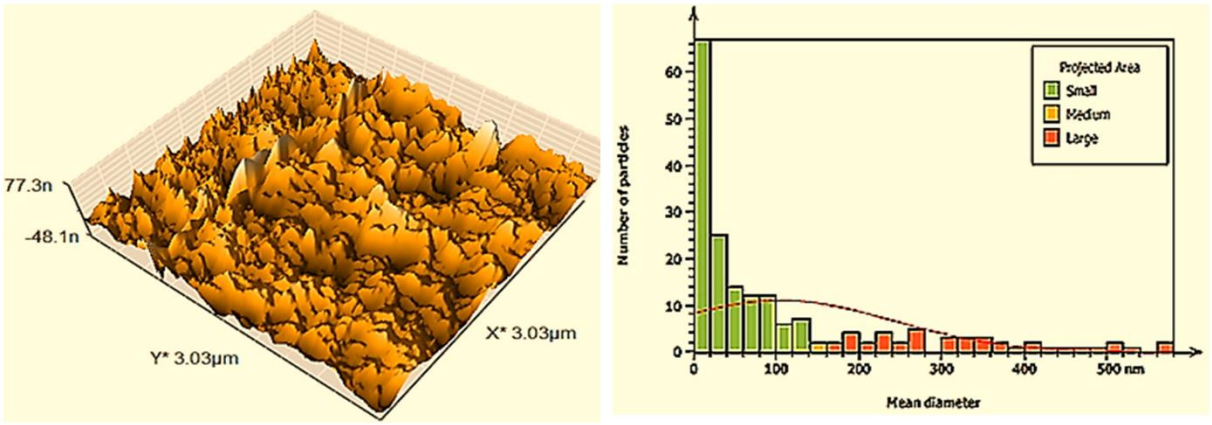


**Figure 17.** AFM image of silica aerogel doped with fluorescein

### 3.5. FESEM images

The FESEM of metal ions copper chloride and silver chloride are shown in figure. 18 a and b, the microscopic structure of the produced aerogels shown in Figure. suggests that metal ions altered the nanoparticles' surface shape, crystal size, and aggregation process. Therefore, the SEM pictures suggest that one of the elements impacting the surface shape of the precursors was ion incorporation. So as to generate an aerogel with sufficient density (from the solution's reactants), the samples were subjected to gelling and curing. When the wet gel was dried, the surface tension was decreased by replacing the pore liquid inside the gel with ethanol. After that, the gels were air-dried to final form. In the end, the resultant organic aerogels were pyrolyzed at a higher temperature [32]. Figures 18, c and d indicate FESEM of coumarin and fluorescein the shape and structure of the pores in TMCS-modified silica beads using scanning electron micrographs. The silica beads, in general, aggregated into dense spherical clusters, but the modified silica beads had a very porous structure. Mesopores with a typical pore diameter were found in TMCS/hexane-modified samples. This is because organic alteration of the surface with trimethyl groups caused reversible shrinkage in the wet gel silica after drying [33].

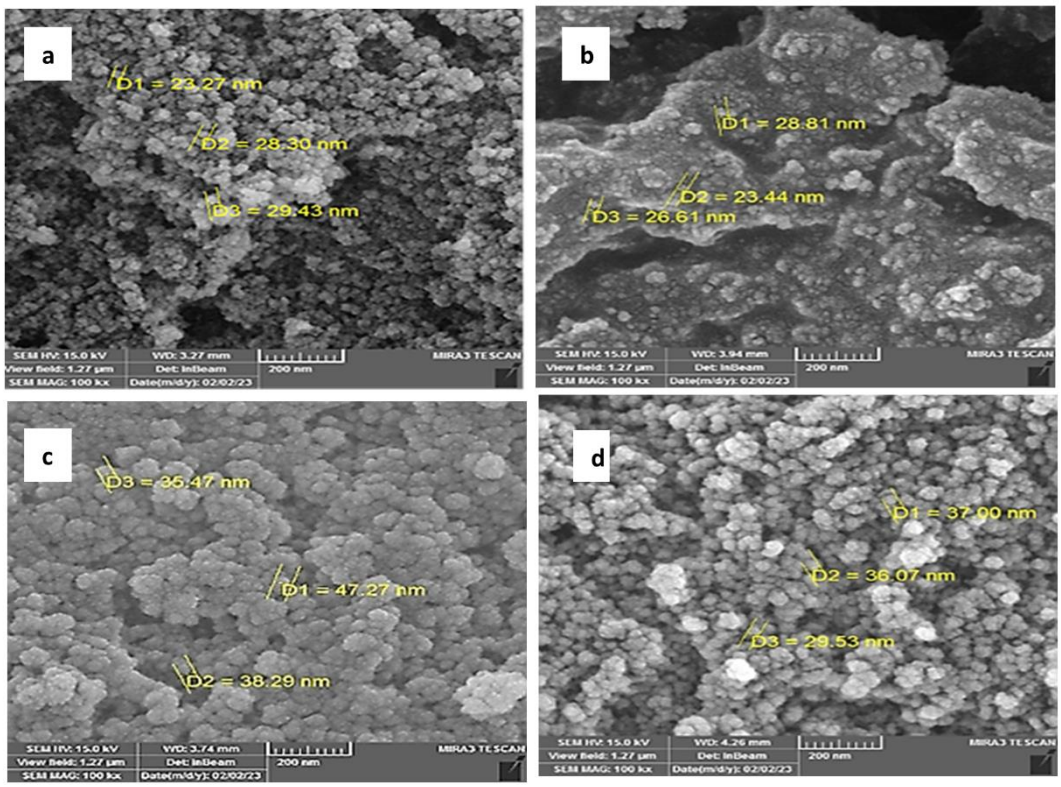


**Figure 18.** FESEM image of silica aerogel doped with a: CuCl, b: AgCl, c: fluorescein, d: coumarin

## 4. Conclusions

The UV absorption shows utmost in the ultraviolet zone and disintegrations in the visible range representing. the FTIR spectrum for the modified sol, gel, aerogel potency necessitated the replacement of hydrophobic (alkyl) for hydrophilic (silanol) groups. Producing and doping nanoparticles using the sol-gel technique. The AFM method was implemented. for a morphological study of these particles. In the event of high the photon will move because of its bands, which means it will hit something when it falls. The effects of fluorescence have shown that the Raman spectrum's peak areas and spread are more different for sol, gel, and aerogel samples. The main reasons are equivalences and nanostructures. There was also microstructural changeability and particle size spreading with a mean significantly different from the residue. FESEM images represented the homogenies and soft stricture in all produced samples and the modified silica beads had a very porous structure. Mesopores with a typical pore diameter were found in TMCS/hexane-modified samples.

## References

[1] B.T. Mekonnen, W. Ding, H. Liu, S. Guo, X. Pang, Z. Ding, M.H. Seid, Preparation of aerogel and its application progress in coatings: A mini overview. Journal of Leather Science and Engineering, 3, (2021) 1-16. https://doi.org/10.1186/s42825-021-00067-y

[2] A. Feinle, M.S. Elsaesser, N. Huesing, Sol–gel synthesis of monolithic materials with hierarchical porosity. Chemical Society Reviews, 45(12), (2016) 3377-3399. https://doi.org/10.1039/C5CS00710K

[3] Y. Wu, D. Ju, H. Wang, H. Zhao, C. Sun, Y. Wu, B. Guo, Y. Wang, Modification of surface structure and mechanical properties in polyimide aerogel by low-energy proton implantation. Surface and Coatings Technology, 403, (2020) 126364. https://doi.org/10.1016/j.surfcoat.2020.126364

[4] Q. Wang, D. Mahadik, P. Meti, Y.-D. Gong, K.-Y. Lee, H.-H. Park, Dioxybenzene-bridged hydrophobic silica aerogels with enhanced textural and mechanical properties. Microporous and Mesoporous Materials, 294, (2020) 109863. https://doi.org/10.1016/j.micromeso.2019.109863

[5] M. Rohaniyan, A. Davoodnia, S.A. Beyramabadi, A. Khojastehnezhad, Phosphomolybdic acid supported on Schiff base functionalized graphene oxide nanosheets: Preparation, characterization, and first catalytic application in the multi-component synthesis of tetrahydrobenzo [a] xanthene-11-ones. Applied Organometallic Chemistry, 33(5), (2019) e4881. https://doi.org/10.1002/aoc.4881

[6] S.S. Ahmed, I.F. Al-Sharuee, superhydrophobic silica monolithic doped with crystal violet dye under ambient pressure: preparation and characterization. New Materials, Compounds and Applications, 6(3), (2022) 282-293.

[7] M.H. Falsafi, M. Moghaddas, J. Moghaddas, Removal of heavy metals from synthetic wastewater using silica aerogel-activated carbon composite by adsorption method. Journal of Applied Research in Water and Wastewater, 7(1), (2020) 90-96. https://doi.org/10.22126/arww.2020.3512.1093

[8] I.F. Al-Sharuee, Thermal conductivity performance of silica aerogel after exposition on different heating under ambient pressure. Baghdad Science Journal, 16(3), (2019) 770-774.

[9] J.L. Gurav, I.-K. Jung, H.-H. Park, E.S. Kang, D.Y. Nadargi, Silica aerogel: synthesis and applications. Journal of Nanomaterials, 2010, (2010) 1-11. https://doi.org/10.1155/2010/409310

[10] J.P. Randall, M.A.B. Meador, S.C. Jana, Tailoring mechanical properties of aerogels for aerospace applications. ACS applied materials & interfaces, 3(3), (2011) 613-626. https://doi.org/10.1021/am200007n

[11] M. Dowson, M. Grogan, T. Birks, D. Harrison, S. Craig, streamlined life cycle assessment of transparent silica aerogel made by supercritical drying. Applied Energy, 97, (2012) 396-404. https://doi.org/10.1016/j.apenergy.2011.11.047

[12] H. Maleki, Recent advances in aerogels for environmental remediation applications: A review. Chemical Engineering Journal, 300, (2016) 98-118. https://doi.org/10.1016/j.cej.2016.04.098

[13] A. Slosarczyk, Synthesis and characterization of silica aerogel-based nanocomposites with carbon fibers and carbon nanotubes in hybrid system. Journal of Sol-Gel Science and Technology, 84, (2017) 16-22. https://doi.org/10.1007/s10971-017-4470-4

[14] H. Maleki, N. Hüsing, Current status, opportunities and challenges in catalytic and photocatalytic applications of aerogels: Environmental protection aspects. Applied Catalysis B: Environmental, 221, (2018) 530-555. https://doi.org/10.1016/j.apcatb.2017.08.012

[15] D. Bokov, A. Turki Jalil, S. Chupradit, W. Suksatan, M. Javed Ansari, I.H. Shewael, G.H. Valiev, E. Kianfar, Nanomaterial by sol-gel method: synthesis and application. Advances in Materials Science and Engineering, 2021, (2021) 1-21.

[16] H. Maleki, L. Duraes, A. Portugal, Development of mechanically strong ambient pressure dried silica aerogels with optimized properties. The Journal of Physical Chemistry C, 119(14), (2015) 7689-7703. https://doi.org/10.1021/jp5116004

[17] M.A. Anaad, I.F. Al-Sharuee, raman spectroscopy and structural characteristics of fluorescein and coumarin doped silica sol, gel, and aerogel. New Materials, Compounds and Applications, 7(2), (2023) 122-136.

[18] S. Salimian, A. Zadhoush, M. Naeimirad, R. Kotek, S. Ramakrishna, A review on aerogel: 3D nanoporous structured fillers in polymer-based nanocomposites. Polymer Composites, 39(10), (2018) 3383-3408. https://doi.org/10.1002/pc.24412

[19] M.H. Sorour, H.A. Hani, G.A. Al-Bazedi, A. El-Rafei, Hydrophobic silica aerogels for oil spills clean-up, synthesis, characterization and preliminary performance evaluation. Journal of Porous Materials, 23, (2016) 1401-1409. https://doi.org/10.1007/s10934-016-0200-5

[20] I.F. Al-Sharuee, Specifications study of hydrophobic silica aerogel doped with rhodamine 6g prepared via sub-critical drying technique. Iraqi Journal of Science, 62(2), (2021) 483-489. https://doi.org/10.24996/ijs.2021.62.2.14

[21] C. Daniel, S. Longo, R. Ricciardi, E. Reverchon, G. Guerra, Monolithic nanoporous crystalline aerogels. Macromolecular rapid communications, 34(15), (2013) 1194-1207. https://doi.org/10.1002/marc.201300260

[22] S.S. Ahmed, I.F. Al-Sharuee, Comparison of the properties of silica aerogel doped with two different laser dyes: Crystal violet and Rhodamine B. Kuwait Journal of Science, 50(3), (2023) 1-15. https://doi.org/10.48129/kjs.20549

[23] W.H. Al-Husseny, I.F. Al-Sharuee, B.R. Ali, spectral and structural analysis for sodium silicate-based aerogel via normal drying pressure. Malaysian Journal of Science, 42(2), (2023) 47-55. https://doi.org/10.22452/mjs.vol42no2.7

[24] I. Al-Sharuee, B.R. Ali, Absorption Spectrum and Raman Spectroscopy of Coumarin507 Dye Laser in Different Solvents. in Diffusion Foundations and Materials Applications, 32, (2023) 45-51. https://doi.org/10.4028/p-03l7q1

[25] L.V. Jathar, M. Kulkarni, D. Himatsinghani, N. Ajwani, D.G. Achalawat, Comparative Study of Coumarin-120 (C-120) and Stilbine-3 (STB-3) Laser Dyes Doped in Sol-Gel Glasses. New Journal of Glass and Ceramics, 11(3), (2021) 57-82. https://doi.org/10.4236/njgc.2021.113004

[26] T.A. Esquivel-Castro, M. Ibarra-Alonso, J. Oliva, A. Martínez-Luévanos, Porous aerogel and core/shell nanoparticles for controlled drug delivery: A review. Materials Science and Engineering: C, 96, (2019) 915-940. https://doi.org/10.1016/j.msec.2018.11.067

[27] W.H. Al-Husseny, I.F. Al-Sharuee, B.R. Ali, water glass based superhydrophobic silica aerogel in different environmental of preparation. New Materials, Compounds and Applications, 6(2), (2022) 127-139.

[28] F.H. Mohammed, I.F. Al-Sharuee, Spectral

examination of erbium dissolved in distilled water at different pH and concentrations. in AIP Conference Proceedings, 2591, (2023). https://doi.org/10.1063/5.0119520

[29] Z. Chen, Y. Zhao, X. Zhu, Inclusion of hydrophobic liquids in silica aerogel microparticles in an aqueous process: microencapsulation and extra pore creation. ACS Applied Materials & Interfaces, 13(10), (2021) 12230-12240. https://doi.org/10.1021/acsami.1c00205

[30] Z. Al-Mothafer, I. Abdulmajeed, I. Al-Sharuee, Effect of oxalic acid as a catalyst and dry control chemical additive (dcca) for hydrophilic aerogel base sodium silicate by ambient pressure drying. Journal of Ovonic Research, 17(2), (2021) 175-183. https://doi.org/10.15251/JOR.2021.172.175

[31] B. Merillas, A. Lamy-Mendes, F. Villafañe, L. Durães, M.A. Rodríguez-Pérez, Silica-Based Aerogel Composites Reinforced with Reticulated Polyurethane Foams: Thermal and Mechanical Properties. Gels, 8(7), (2022) 392. https://doi.org/10.3390/gels8070392

[32] A.V. Rao, Elastic superhydrophobic and water glass-based silica aerogels and applications. Journal of Sol-Gel Science and Technology, 90, (2019) 28-54. https://doi.org/10.1007/s10971-018-4825-5

[33] P. Veres, G. Király, G. Nagy, I. Lazar, I. Fábián, J. Kalmár, Biocompatible silica-gelatin hybrid aerogels covalently labeled with fluorescein. Journal of Non-Crystalline Solids, 473, (2017) 17-25. https://doi.org/10.1007/s10971-018-4825-5

## Acknowledgments

The authors would like to thank Mustansiriyah University and Chemistry Analysis Center for their laboratory tests for their valuable support.

## Authors Contribution Statement

Mohammed A. Anaz: Experimental, Formal analysis, Writing—original draft preparation, Writing, Review and editing, Israa F. Al-sharuee: conceptualization, methodology, software, validation, Writing, Review and editing.

## Funding

The Manuscript was funded solely by the Participating Researchers.

## Competing Interests

The authors declare that there are no conflicts of interest regarding the publication of this manuscript.

## Data Availability

Data and materials related to the research work will be available based on the request.

## Has this article screened for similarity?

Yes

## About the License